

Mechanism of Enhanced Fracture Toughness in a Novel Al-Cu-Li-Ce Alloy

Yu Xinxiang, Yin Dengfeng, Yu Zhiming, Wang Jing, Cui Fan

Central South University, Changsha 410083, China

Abstract: The effects of different cerium contents on the mechanical properties of a novel Al-Cu-Li alloy under the peak aged conditions of T6 and T8 were studied by conventional tensile test and Kahn Tear Test. In addition, the grain boundary precipitates and fractography were observed by transmission electron microscopy (TEM) and scanning electron microscope (SEM). The results show that the UIE and the strength for alloys under T6 condition are generally lower than those for the alloys under T8 condition, while strength-toughness combination has been obtained in alloy 2#(0.15% Ce) under T8 (pre-stretched + artificially aged) condition. Meanwhile, a statistic analysis of the microscopic data by Image-Pro Plus (IPP) software, taking into account the effect of cerium content and pre-stretch was carried out. The analysis shows that the larger area fraction of the combination of dimples and intermetallic particles is corresponding to the higher value of UIE. The changes in the precipitate free zone (PFZ) width, grain boundary precipitate number density and grain boundary precipitate effective size govern the fracture resistance and the crack path of the test alloy under the conditions of the different Ce contents and heat treatment.

Key words: Al-Cu-Li alloy; Ce element; UIE; brittle intergranular fracture; grain boundary precipitate

Fracture toughness is a crucial material design criterion for many high strength materials applications^[1]. Al-Cu-Li based alloys can reach extremely high strength through a fine scale precipitate dispersion composed mostly of high-aspect ratio plate-like T_1 (Al_2CuLi) precipitates (2 nm thick), inhabiting the {111} planes. It can hinder the {111} aluminium matrix plane slip effectively^[2-4]. By comparison with conventional aluminium alloys, the present generation of Al-Cu-Li based alloys has some unsatisfactory sides in mechanical characteristics such as ductility and fracture toughness^[5-7]. However, there is much interest in further improving the strength-ductility combination in Al-Cu-Li based alloys for aerospace applications^[8]. One of the main reasons why Al-Cu-Li based alloys have lower ductility and fracture toughness is that a coarse lithium containing phase precipitate at grain boundary promotes intergranular fracture readily^[9-12].

The use of rare earth cerium as a micro-alloying element

in Al has been studied for several years. The mechanical properties of the Al-Li-Mg alloys were improved and the negative effect of impurity Fe was controlled by Ce addition. The Ce addition was also reported to affect the ductility and fracture toughness of 8090 alloy sheets rich in impurities of Fe, Si and alkali metals^[13].

The delamination cracking in advanced aluminium-lithium (Al-Li) alloys plays a dominant role in the fracture process. With the introduction of these materials into components of aerospace structures, a quantitative understanding of the interplay between delamination cracking and macroscopic fracture must be established as a precursor to reliable design and defect assessment^[14].

The use of precipitation strengthened Al-Cu-Li based alloys with small cerium addition will therefore require better understanding of the related mechanisms of microstructural evolution and optimizing property. The objective of the present study is to assess the effect of cerium content on the

Received date: May 23, 2013

Foundation item: Research Foundation of the General Armament Department (6140506)

Corresponding author: Yin Dengfeng, Ph. D., Associate Professor, School of Materials Science and Engineering, Central South University, Changsha 410083, P. R. China, Tel: 0086-731-88879341, E-mail: dfyin@126.com

Copyright © 2014, Northwest Institute for Nonferrous Metal Research. Published by Elsevier BV. All rights reserved.

fracture property of a novel Al-Cu-Li alloy and relate those properties to the fracture pattern and the grain boundary precipitate.

1 Experiment

The chemical compositions of the alloys used in this experiment are shown in Table 1.

Master alloys of Al-Zr, Al-Ce and Al-Cu and pure elements of Ag, Mg, Li and Al were melted in a vacuum induction melting furnace under controlled atmosphere of argon gas, using high pure graphite crucible. Lithium addition was made by plunging Li wrapped in aluminium foil. Casting was carried out under argon. The cast ingots were homogenized at 450 °C for 16 h followed by treating at 500 °C for 8 h in a salt bath furnace prior to be hot and cold rolled to 2 mm from 23 mm in thickness. Samples were solution-treated at 520 °C for 0.5 h, artificially aged at 180 °C (peak-aged) for T6 and artificially aged at 150 °C (peak-aged) for T8.

The strength was measured by conventional tensile tests, the tear resistance was measured on Kahn Tear Test method (three samples for each test), the relevant parameter was the unit initiation energy as UIE (the energy dissipated before crack propagation), and the alloys were tested in the *L-T* direction. Fractography of all three alloys were observed by scanning electron microscope (SEM). The composition of large secondary particles was measured by energy dispersive X-ray (EDX) analyzer. A statistic analysis of the area fraction of both brittle intergranular (IG) fracture and combination of dimples and intermetallic particles on all conditions were carried out by Image-Pro Plus (IPP) software.

Transmission electron microscopy (TEM) was applied to characterize the microstructures of the alloys with different Ce additions. TEM samples were electrically polished in a 70% carbinol and 30% nitric acid solution at -35 °C, using a twin-jet equipment operated at 30 V.

2 Results

2.1 Mechanical property

The effects of cerium contents on the strength and the value of UIE at peak aged are illustrated in Fig.1. Fig.1 shows that tensile strength (σ_b and $\sigma_{0.2}$) for T6 temper first decreases and then increases with the increase of cerium content, while the behavior of tensile strength (σ_b and $\sigma_{0.2}$) for T8 temper keeps almost the same. There is no apparent change when the Ce content increases from 0 to 0.3 %.

Fig.1 also shows that the value of UIE for T6 temper increases linearly with the increase of cerium content. In general, the UIE and strength for alloys under T6 condition are lower than those for the alloys under T8 condition. Particularly, UIE is the highest for alloy 2# (0.15%Ce) arti-

Table 1 Measured chemical composition of alloy (wt%)

Alloy No.	Ce	Li	Cu	Mg	Ag	Zr	Al
1#	-	1.29	1.59	0.4	0.4	0.14	Bal.
2#	0.14	1.33	1.56	0.4	0.4	0.14	Bal.
3#	0.29	1.31	1.58	0.4	0.4	0.14	Bal.

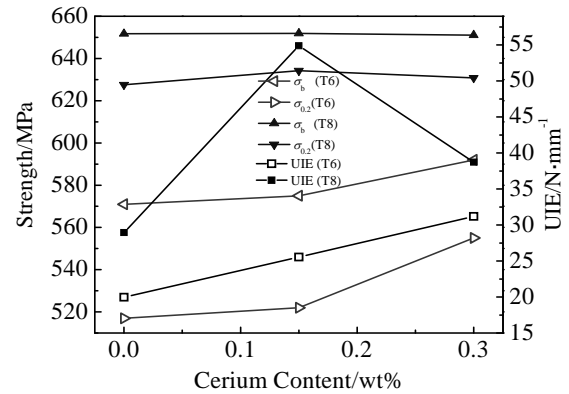


Fig.1 Plots of strength and UIE versus cerium content under T6 and T8 conditions

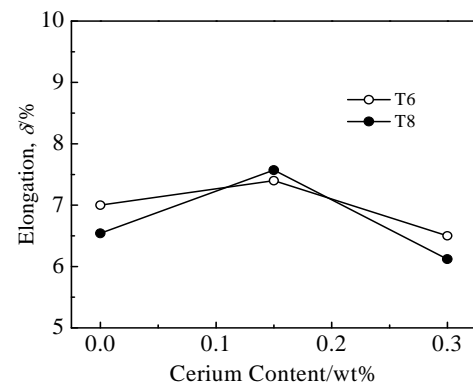


Fig.2 Plots of elongation versus cerium content under T6 and T8 conditions

cially aged at T8. Furthermore, as is observed in Fig. 2, the highest value of elongation is obtained in alloy 2#. Thus, strength-toughness combination can be obtained in alloy 2# under T8 condition.

2.2 Optical micrograph

Optical micrographs of T6 (a~c) and T8 (d~f) heat treated samples are shown in Fig.3. A fully recrystallised grain structure is presented in all six samples, while an even more finer and uniform equiaxed grains are presented in the high (0.3%) Ce alloy under T6 condition (Fig.3c). On the other hand, larger grains are presented in the no Ce containing alloy under T6 condition (Fig.3a). Moreover, the grain size for three alloys under T8 condition is almost the same.

2.3 Fractography

Fractographs of all three alloys under T6 (a~c) and T8 (d~f) conditions are shown in Fig.4. The fractograph of alloy 1# shows that a predominantly brittle island (brittle grain boundary fracture) is surrounded by dimples when the

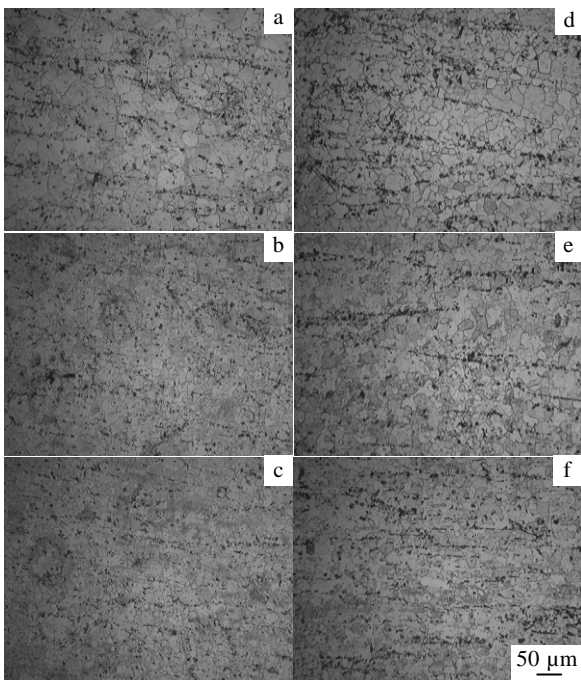


Fig.3 Optical micrographs of all three alloys under T6 (a-c) and T8 (d-f) conditions: (a, d) alloy 1#; (b, e) alloy 2#; (c, f) alloy 3#

fracture occurs along the boundaries of recrystallised grains. That can topographically resemble a brittle intergranular fracture, even though at low magnification it appears as a smooth fracture. The size and the area fraction of the brittle island for alloy 1# are very large, which decrease with increasing of Ce content to a level of 0.3%.

Delaminations characteristic is obvious under T8 condition as compared to the fractographs under T6 condition. It is a kind of brittle fracture which is contributed to the fracture toughness enhanced compared with pure brittle fracture. Microvoid coalescence surrounding the particles is also seen under all conditions. The respective area fractions of the fracture modes have been quantitatively measured on a large number of SEM images.

The SEM study results of grain fracture mode in the test alloys are shown in Table 2 and Table 3. As can be seen in Table 2, the area fraction of smooth brittle intergranular fracture decreases rapidly with increasing of cerium content. Meanwhile, the area fraction of combination of dimples and intermetallic particles rise with increasing of cerium content. SEM studies of fracture mode under T8 condition are also shown in Table 3. However, the highest area fraction of combination of dimples and intermetallic particles is for alloy 2# with cerium content just 0.15%.

2.4 Grain boundary precipitate

Fig.5 are bright-field TEM images of grain boundaries from three materials under T6 and T8. The grain bound-

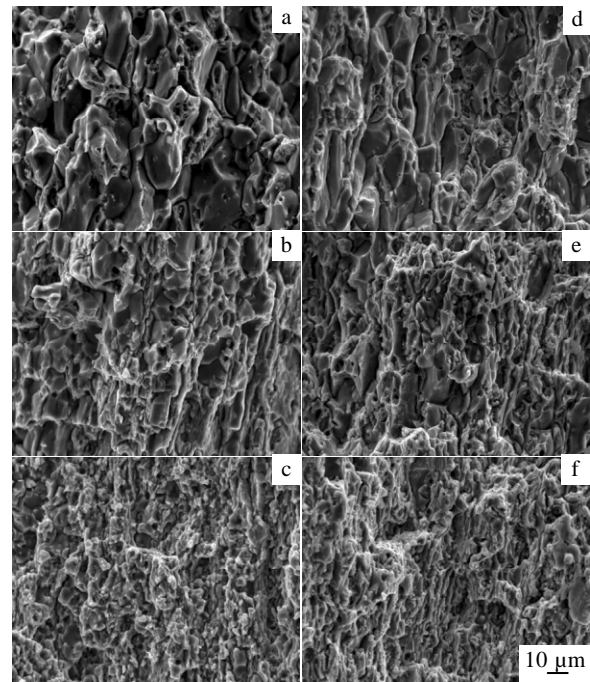


Fig.4 Fractography of all three alloys under T6 (a-c) and T8 (d-f) conditions: (a, d) alloy 1#; (b, e) alloy 2#; (c, f) alloy 3#

Table 2 SEM study results of fracture mode under T6 condition

Alloy No.	BGBF*			A _d */%
	Mean area/μm ²	Number density/μm ²	Area fraction/%	
1#	391	42	85.50	14.50
2#	116	61	37.90	62.10
3#	24	117	15.04	84.96

*BGBF: brittle grain boundary fracture, A_d: area fraction of dimples and intermetallic particles

Table 3 SEM study results of fracture mode under T8 condition

Alloy No.	BGBF*/%	AD*/%	TD*/μm	A _d */%
1#	60.62	14.49	8.57	24.89
2#	21.29	19.28	2.61	40.57
3#	9.18	24.89	2.14	34.07

*BGBF: brittle grain boundary fracture, AD: area fraction of delamination, TD: thickness of delamination, A_d: area fraction of dimples and intermetallic particles

ary precipitates have a blockier morphology (lower aspect ratio) compared to those precipitated in the matrix.

TEM studies of the grain boundary regions of three alloys were performed. Several parameters pertaining to the grain boundary precipitates were determined including: (1) the number of precipitates per unit grain boundary area (*N*); (2) effective sizes of grain boundary precipitates, expressed as $(\text{Length} \times \text{width})^{1/2}$ (*D*); (3) half-width of the precipitate free zone (*W*)^[15].

The transmission electron microscopy study results of grain boundary precipitation in the test alloys are shown

in Table 4 and Table 5. In particular, there are two kinds of particles in the grain boundary for alloy 3 # under T6 condition.

3 Discussion

The differences in cerium content, grain size, the pre-

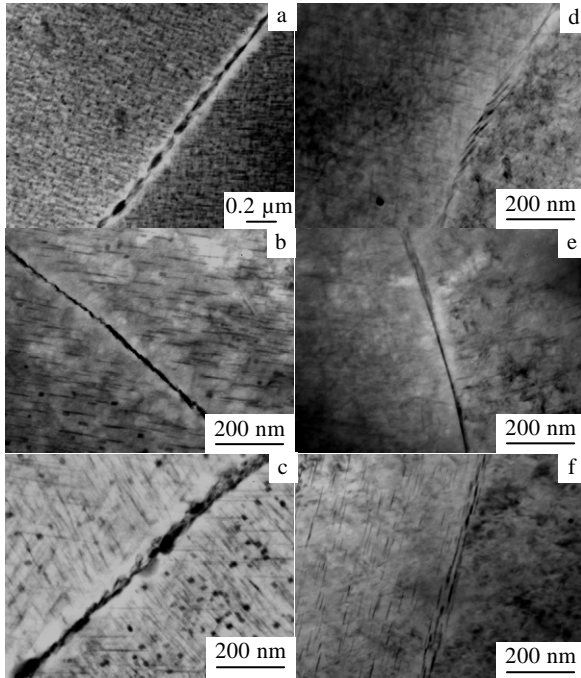


Fig.5 Grain boundary precipitation of all three alloys under T6 (a-c) and T8 (d-f) conditions: (a, d) alloy 1#; (b, e) alloy 2#; (c, f) alloy 3#

Table 4 TEM study results of grain boundary precipitation under T6 condition

Alloy No.	$W^*/\mu\text{m}$	$D^*/\mu\text{m}$	$N^*/\mu\text{m}^{-2}$	ε_f/k^n	E_f^*
1#	0.052	0.0780	44	2.51	1.58
2#	0.063	0.0357	177	7.87	2.80
3#	0.030	0.0199	311	12.2	3.5
		0.044	70	5.03	2.24

W : 1/2 PFZ (precipitate free zone) width, D : effective diameter, N : number density, E_f : $(\varepsilon_f/k^n)^{1/2}$

Table 5 TEM study results of grain boundary precipitation under T8 condition

Alloy No.	$W^*/\mu\text{m}$	$D^*/\mu\text{m}$	$N^*/\mu\text{m}^{-2}$	ε_f/k^n	E_f^*
1#	0.017	0.0223	350	4.380	2.090
2#	0.038	0.0186	149	39.960	6.320
3#	0.035	0.0180	466	12.880	3.590

W : 1/2 PFZ (precipitate free zone) width, D : Effective diameter, N : Number density, E_f : $(\varepsilon_f/k^n)^{1/2}$

cipitate behavior in grain and grain boundary structure would be to influence fracture toughness to some extent.

3.1 Effect of cerium and pre-stretch on strength

The effects of the trace addition of cerium on the microstructural evolution and the mechanical properties of this novel Al-Cu-Li alloys were investigated in another paper^[16]. According to these results, the microstructure in this research is consist of three kinds of precipitates such as T_1 phase (Al_2CuLi), θ' phase (Al_2Cu) and cubic phase ($\text{Al}_2\text{Cu}_6\text{Li}$). TEM results indicate that the total nucleation sites increase with the enhanced content of cerium. The uniformity in size for θ' phase is different in alloy 1# and 2#, and it is attributed to the competitive precipitation between cubic phase and θ' phase in alloy 1#. The enhancing of T_1 phase size in alloy 3# directly correlates with the marked increase in the number density of T_1 nucleation sites. It can be concluded that the dissolution of cubic phase occurs in alloy 2# during the initial aging, while the reprecipitation and the growth of T_1 phase happen immediately.

As the trace addition of cerium, it would be exist in the form of solid solution and distributed at $\{100\}$ matrix face and $\{111\}$ matrix face, respectively. The increase in density for the cubic phase and T_1 phase between different cerium contents are attributed to the introduction of heterogeneous matrix nucleation sites at $\{100\}$ matrix face and $\{111\}$ matrix face separately. In addition, the trace cerium element is thought to tie up vacancies and limit the Cu diffusion which is necessary for GP zone formation and θ' precipitate at last. Hence the strength rises with the increasing of content of cerium at peak aged under T6 condition.

Plastic deformation prior to artificial aging in three alloys has been found to enhance the strength, the ductility and aging kinetics over non-deformed materials through the introduction of the dislocations, which act as preferential matrix nucleation sites for the primary strengthening phase T_1 . The same amount of introduced plastic deformation in three alloys leads to the same number of matrix dislocations. Therefore, the effect of cerium is very small and the strength is almost the same at peak aged under T8 condition.

3.2 Effect of cerium and pre-stretch on grain size

It was reported that the Ce content affected the grain size of a binary Al-Li alloy^[13]. Increasing cerium content was known to decrease grain size of Al-Li alloys, which might result in higher value of fracture toughness. Under T8 condition, a large number of dislocations are incorporated by cold work, which act as the preferential nucleation site of recrystallization. Thus cerium content does not appear to have significant effects on the grain size. The examination of the grain size and the value of UIE suggest that there is no major effect of the grain size on the fracture toughness for the materials treated under

T6 and T8 conditions.

3.3 Effect of cerium and pre-stretch on fracture mode

The statistic analysis of the effect of Ce content and pre-stretch suggests that there is a beneficial effect on fracture toughness with large area fraction of combination of dimples and intermetallic particles, shown in Fig.6. The area fraction of combination of dimples and intermetallic particles (A_d) are normalized by the T6 with cerium content of 0.3% and T8 with cerium content of 0.15%, respectively.

Planar slip is always exhibited in conventional aluminum-lithium alloy, which is due to shearing of the coherent and ordered δ' precipitates, leading to slip concentration. Once a critical strain is reached in these crystallographic deformation bands, fracture will occur in a crystallographic mode^[17]. Under the conditions of a high Cu/Li ratio and the Li content just with 1.3 wt%, the only strengthening precipitates existing here on the peak-aged conditions are the T_1 θ' and cubic phase ($Al_5Cu_6Li_2$)^[18]. Because of the absence of δ' precipitates in this alloys, the planar slip mode may arise from GP-zones at the underaged conditions. The planar slip mode brings about crystallographic cracking as noted previously in a high purity Al-Cu alloy^[19]. As the GP-zone decreases with adding cerium content on T6, thus the area of brittle grain boundary fracture (BGBF) also decreases on T6 condition. In addition, pre-age plastic deformation enhances the aging kinetics, the strength and the number density of fine strengthening precipitates through the introduction of heterogeneous matrix nucleation sites. Compared to the alloy with no Ce content, the relative volume fraction of T_1 to θ' greatly increases with the adding of Ce, the planar slip mode arising from GP-zones decreases with the adding of Ce. However, for the cerium containing alloy (2#, 3#), because a large number of vacancy is trapped in dislocation, the effect of cerium element tying up vacancies and limiting the Cu diffusion which is necessary for GP zone formation is small. On the other hand, Fig.7 shows that overmuch Ce content results in coarsening precipitates which might be harmful to fracture toughness. On the contrary, alloy 2# under T8 condition has the largest area fraction of combination of dimples and intermetallic particles corresponding to the highest fracture toughness.

3.4 Effect of cerium and pre-stretch on grain boundary characteristic

The strength of the alloy reaches a maximum under peak aged condition. With the strength increasing, the plasticity of the alloy decreases. Under these conditions, the fracture process becomes brittle, here the brittle fracture is mostly due to grain boundary precipitates formed during aging treatment. Moreover, the principal reason for the incidence of grain boundary fracture is dominated

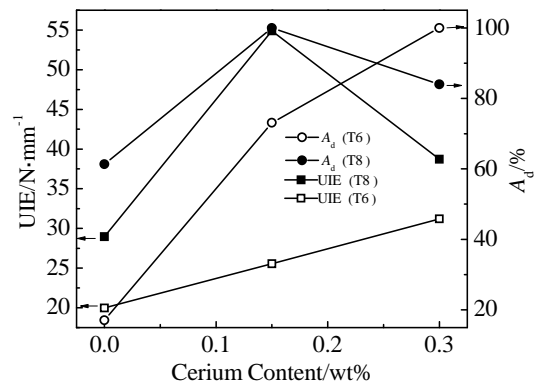


Fig.6 Plots of A_d and UIE versus cerium content under T6 and T8 conditions

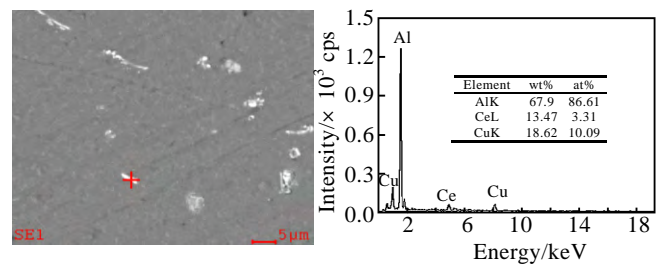


Fig.7 EDX image of residual phases of alloy 3#

by the spacing and the size of void nucleating particles on the boundaries with strain localization in the PFZ. The following equation^[20] for determination of grain boundary fracture may be plausible :

$$\epsilon_f = k^n W / (D^3 N) \quad (1)$$

where ϵ_f is the grain boundary fracture strain, and k^n is a constant. The grain boundary fracture strains were calculated using this equation and the values are shown in Table 4 and Table 5. The grain boundary fracture strains (calculated using this equation) raised to the one-half power are plotted in Fig.8. As can be seen in Fig.8, E_f [$(\epsilon_f/k^n)^{1/2}$] and UIE exhibit similar dependence on cerium content both under the T6 and T8 conditions.

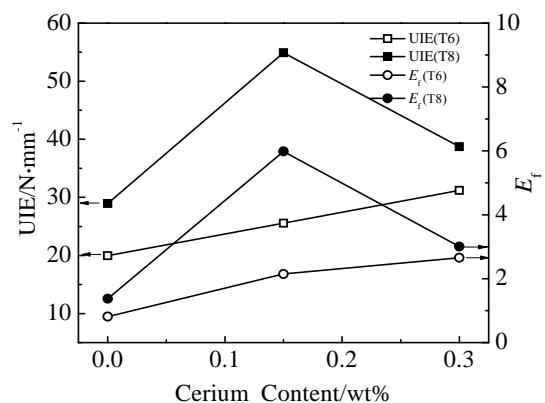


Fig.8 Plots of E_f and UIE versus cerium content on T6 and T8 conditions

The high concentration and the significant vacancy binding energy of Ce atoms cause the preferential clustering between Ce atoms and quench-in vacancies, then the diffusion of Cu, Li atoms is retarded and therefore the nucleation of Cu or Li-rich phases in grain boundaries is suppressed. On the contrary, cerium content does not have significant effects on toughness for the material with plastic deformation prior to artificial aging (T8), which could be explained on the basis that cerium is presented as coarse precipitate or being trapped in dislocation rather than as retarding solute segregate to grain boundary.

4 Conclusions

1) With increasing of cerium content under T6 condition, the planar slip mode arising from GP-zones decreases, the area of brittle grain boundary fracture (BGBF) and decreases.

2) Comparing with the no Ce containing alloy (1#) under T8 condition, the relative volume fraction of T_1 to θ' (GP-zones) greatly increases with adding of Ce, the planar slip mode arising from GP-zones decrease.

3) For the cerium containing alloy (2#, 3#) under T8 condition, the effect of cerium element tying up vacancies and limiting the Cu diffusion which is necessary for GP zone formation is small. on the other hand, overmuch Ce content results in coarsening precipitates which might be harmful to fracture toughness.

4) The increase of fracture toughness is associated with the area fraction of combination of dimples and intermetallic particles both under the T6 and T8 conditions. Strength-toughness combination can be obtained in alloy 2 (0.15% Ce) under T8 condition which has the highest area fraction of combination of dimples and intermetallic particles.

5) The high concentration and the significant vacancy binding energy of Ce atoms cause the preferential clustering between Ce atoms and quench-in vacancies, resulting in retarding the diffusion of Cu, Li atoms, and suppressing the nucleation of Cu or Li-rich phases at grain boundaries under T6 condition.

References

- Morgeneyer T F, Starink M J, Sinclair I. *Acta Materialia*[J], 2008, 56: 1671
- Yoshimura R, Konno T J, Abe E et al. *Acta Materialia* [J], 2003, 51: 4251
- Murayama M, Hono K. *Scripta Materialia*[J], 2001, 44: 701
- Gault B, Geuser F, Bourgeois L et al. *Ultramicroscopy*[J], 2011, 111: 207
- Wanhill R J H. *Int J Fatigue*[J], 1994, 16: 3
- Prasad N E, Kamat S V, Malakondaiah G et al. *Fatigue Fract Eng Mater Struct*[J], 1994, 17: 441
- Gayle F W, Tack W T, Swanson G et al. *Scr Metall Mater*[J], 1994, 30: 761
- Lavernia E J, Grant N J. *J Mater Sci*[J], 1987, 22: 1521
- Hornbogen E, Starke E A. *Acta Metall Mater*[J], 1993, 41: 1
- Webster D. *Adv Mater Process*[J], 1994, 145: 18
- Blankenship C P, Starke E A. *Metall Trans A*[J], 1993, 24: 833
- Feng W X, Lin F S, Starke E A. *Metall Trans A*[J], 1984, 15: 1209
- Xiao D H, Wang J N, Ding D Y et al. *Journal of Alloys and Compounds*[J], 2003, 352: 84
- Kalyanam S, Beaudoin A J, Dodds J R H et al. *Engineering Fracture Mechanics*[J], 2009, 76: 2174
- Reynolds A P, Li Qiong. *Scripta Materialia*[J], 1996, 34: 1803
- Yu X X, Yu Z M, Ying D F et al. *Rare Metal Materials and Engineering*[J], 2014, 43(2): 495 (in Chinese)
- Jata K V, Starke E A. *Metallurgical and Materials Transactions A*[J], 1986, 17: 1011
- Pan Z R, Zheng Z Q, Liao Z Q et al. *Materials Letters*[J], 2010, 64: 942
- Jata K V, Vasudevan A K. *Materials Science and Engineering: A*[J], 1998, 241: 104
- Liu W H, Zhang X M, Tang J G. *Mechanics of Materials*[J], 2009, 41: 799

新型 Al-Cu-Li-Ce 合金增韧化机制

余鑫祥, 尹登峰, 余志明, 王景, 崔凡
(中南大学, 湖南 长沙 410083)

摘要: 采用室温拉伸和 Kahn 撕裂测试方法, 对一种加入不同含 Ce 量的新型 Al-Cu-Li 合金在 T6 态和 T8 态峰时效时的力学性能分别进行了测试; 同时辅以扫描电镜和透射电镜对其断口形貌和晶界析出相相应的变化规律进行了研究。对所有状态样品的断口扫描照片和晶界析出相情况进行了统计。结果表明: T8 态的强度值和 UIE 值 (unit initiation energy) 总体高于 T6 态, 中等含 Ce 量的合金在 T8 态具有最高的强韧性配合。断口分析中发现: 具有韧窝环绕金属间化合物特征的区域所占面积分数的变化趋势与 UIE 值变化规律一致; 晶界分析表明: 无析出带宽度的大小、晶界析出相的数密度和有效尺寸的变化决定了样品在不同 Ce 含量和热处理状态下的断裂阻力和裂纹扩展方式。

关键词: Al-Cu-Li 合金; 稀土铈; UIE 值; 脆性沿晶断裂; 晶界析出相

作者简介: 余鑫祥, 男, 1984 年生, 博士生, 中南大学材料科学与工程学院, 湖南 长沙 410083, 电话: 0731-88879341, E-mail: 834139001@qq.com